40

Fine Structure and Finer Details

CHAPTER PREVIEW

In the previous chapter, we described elemental analysis using ionization edges, but there is much more than just elemental information in the ionization edges and this distinguishes EELS from XEDS. There are detailed intensity variations in the core-loss spectra called energy-loss near-edge structure (ELNES) and extended energy-loss fine structure (EXELFS). From this fine structure, which we can resolve because of the high-energy resolution inherent in EELS, we can obtain data on how the ionized atom is bonded, the coordination of that specific atom, and its density of states. As always, we can use any intensity changes to create filtered images which show the distribution of, e.g., regions of different bonding states. Furthermore, we can probe the distribution of other atoms around the ionized atom (i.e., determine the radial-distribution function (RDF) which is very useful for the study of amorphous materials) and we can study momentum-resolved EELS, observe the anisotropy of chemical bonds, combine EELS with tomography, inter alia. Understanding these phenomena often requires that we use certain concepts from atomic and quantum physics. The non-physicist can skip some sections at this time and just concentrate on the results. The rewards of working through this topic will be an appreciation of some of the more powerful aspects of EELS.

> **WHY LOOK AT FINE STRUCTURE ?**
> If high spatial resolution is important, you can't obtain this additional information by any other spectroscopic technique.

This fine structure is all the more useful because we now have the ability to simulate the spectra using atomic-structure calculations, which help us understand the details in the spectra. A full appreciation of the calculations is beyond the scope of the book but this is a growing field that will only assume more significance.

As a wrap-up to EELS and the book as a whole, we'll finish by saying a few words on some of the more esoteric aspects of TEM, such as angular-resolved spectrometry, radial-distribution-function determination, Compton scattering, core-level shifts, and tomographic EELS that are not yet in the mainstream but, with continuing advances in instrumentation and computation, will surely grow in importance.

40.1 WHY DOES FINE STRUCTURE OCCUR?

We saw in Section 39.1 that the ionization edges have intensity variations superimposed on the ideal hydrogenic sawtooth shape. The stronger oscillations occur within about 30–50 eV of the onset of the edge (ELNES) and the weaker ones extend out for several hundred eV as the edge intensity diminishes (EXELFS). This fine structure contains a wealth of useful information, but to understand its origins you have to use some ideas from quantum physics.

One way we can look at this process is to switch from a particle to a wave model of the electron, as we've done before, e.g., when we talked about diffraction in Part 2. Then we can imagine that any excess energy ($>E_c$) that the ejected electron possesses is a wave emanating from the ionized atom. Now, if this wave has only a few eV of excess energy, it undergoes plural, elastic scattering from the surrounding atoms, as shown schematically
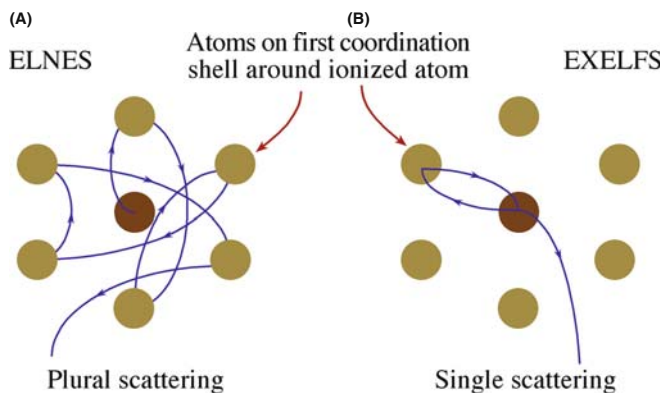
FIGURE 40.1. Schematic diagram showing the source of (A) ELNES and (B) EXELFS. The excess energy retained by the electron escaping above the Fermi level creates a wave radiating from the ionized atom and is scattered by surrounding atoms. The low-energy ELNES arises from plural scatter and is affected by the bonding between the atoms. The higher-energy EXELFS approximates to single scatter and is affected by the local atomic arrangement.

in Figure 40.1A, and this scattering is responsible for the ELNES, as we'll show. If the wave has even more excess energy, then, because of the smaller interaction cross section for higher-energy electrons (as we've already seen many times) it is less likely to be scattered by the surrounding atoms. In fact, we can approximate the cause of the ELNES to a single-scattering event, as shown in Figure 40.1B. Thus, EXELFS and ELNES can be viewed as a continuum of electron-scattering phenomena, with the arbitrary distinction that ELNES is confined to a few tens of eV past the edge onset while EXELFS extends for several hundred eV past the edge onset. There are other ways to explain fine structure and we'll mention some of these later when we talk about modeling the phenomena.

> ### ELNES AND EXELFS I
> Both arise because the ionization process can impart more than the critical ionization energy (E_c) needed by the core electron to be ejected from its inner shell.
> Energy-Loss Near-Edge Structure
> EXtended Energy-Loss Fine Structure

You should know that similar fine-structure effects can occur in X-ray spectra, but are usually not resolvable in the TEM because of the poor resolution of the semiconductor XEDS detector. However, we did note that experimental high-resolution X-ray detectors can resolve bonding effects in terms of shifts in X-ray peaks (see Figure 32.9C). In fact, there is a whole field of X-ray spectrometry that is used for studying atomic bonding (X-ray absorption near-edge structure or XANES) and atom positions and structure (extended X-ray absorption

fine structure or EXAFS). These techniques are analogous to ELNES and EXELFS, but require a synchrotron to generate sufficient signal. This is one of the few examples where TEM is the cheaper characterization technique.

Most of this chapter deals with the experimental measurement and basic theoretical simulation of ELNES and EXELFS; the information we give is augmented in the companion text. While ELNES arises from plural scattering and is thus a more complex process than EXELFS, it is much more widely used, because it gives a more intense signal and the information it reveals has been used to study a very wide range of materials. So we'll discuss ELNES first.

40.2 ELNES PHYSICS

40.2.A Principles

As you know well, when an atom is ionized, it is raised from its ground state to an excited state leaving a hole in an inner shell. The core electron must receive enough energy from the beam electron to be ejected from its shell, but it may not receive enough to escape to the vacuum level. So it is still not completely free of the Coulomb attraction to the nucleus. In such circumstances, the final state of the core electron will be in one of a range of possible energy levels above the Fermi energy (E_F). You may recall that the Fermi level (or the Fermi surface in three dimensions) is the boundary between the filled states and the unfilled states in the weakly bound conduction/valence bands (although, strictly speaking, this statement is only true when $T = 0$ K). In a metal, there is no separate valence band and E_F sits somewhere in the conduction band, as shown schematically in the classic energy level diagram of an atom in Figure 40.2. In an insulator or a semiconductor, E_F is between the valence band (in which all the states are filled) and the conduction band (which has no filled states). The possible energy values that can be imparted to the ejected electron are controlled by the energy distribution of these unfilled states and, therefore, the energy lost by the incident electron similarly reflects this distribution of the unfilled states. One philosophical point of quantum uncertainty is that these states don't exist until an electron appears in them, but we'll conveniently ignore this.

So, the excited electron can reside in any of the unfilled states, but what's crucial here is that there is not an equal probability of the electron ending up in each possible unfilled state. Some empty states are more likely to be filled than others because there are more states within certain energy ranges than in others. This uneven distribution of empty energy levels is termed the density of (unfilled) states (DOS) and this is also shown
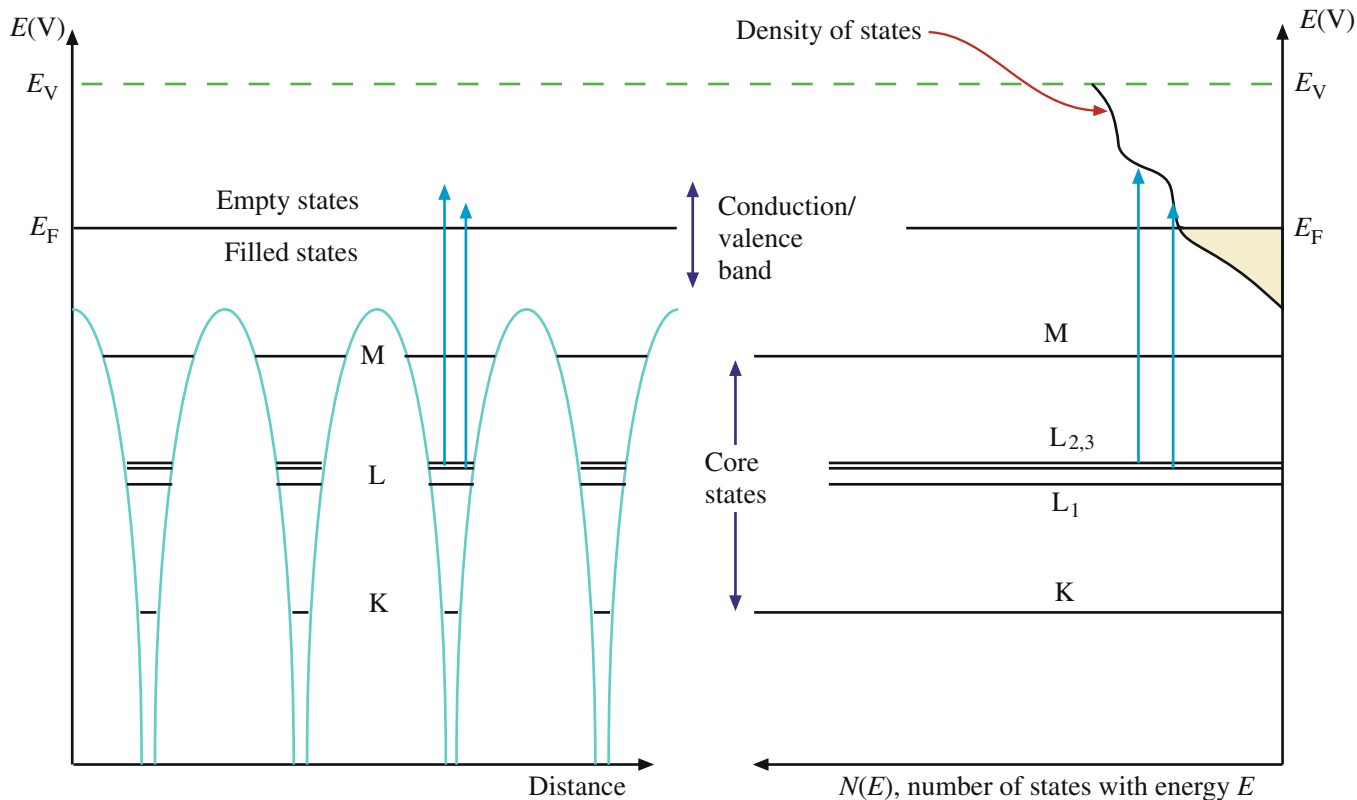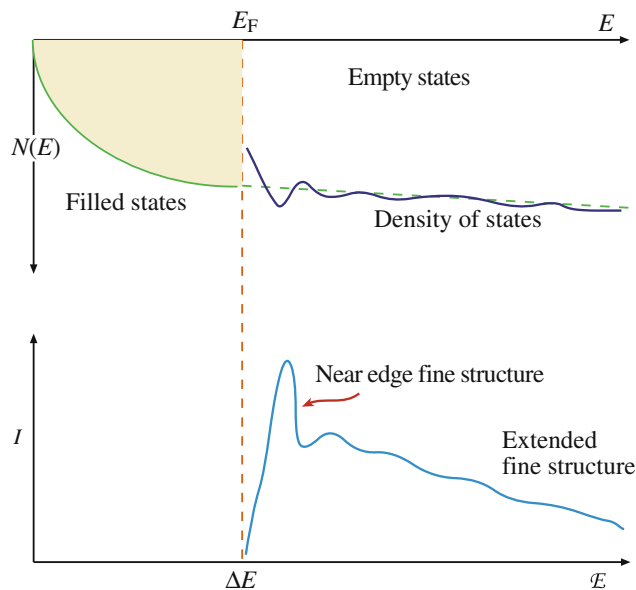
FIGURE 40.2. Relationship between the classic energy diagram of a metal atom (left) and the density of filled (shaded) and empty (unshaded) states in the conduction/valence band (right). The DOS is approximately a quadratic function on which small variations are superimposed. Ionization results in electrons being ejected from the core states into empty states above the Fermi level E_F.

in Figure 40.2. Because of the greater probability of electrons filling certain unoccupied states above E_F, the ELNES intensity is greater at the energy losses corresponding to these high DOS regions above the Fermi energy (which can be thought of as equivalent to the critical ionization energy E_C), as shown in Figure 40.3.

> ### ELNES
> This variation in intensity, extending several tens of eV above the ionization edge onset, E_C, is the ELNES, and it effectively mirrors the unfilled DOS above E_F.

The importance of ELNES is that the DOS is extremely sensitive to changes in the bonding or the valence state of the atom. For example, if you look ahead to Figure 40.5, the carbon K ELNES is different for graphite, diamond, and buckyballs and the Cu L ELNES changes when Cu is oxidized to CuO. On an even more detailed level, we can even deduce the coordination of the ionized atom from the shape of the ELNES.

FIGURE 40.3. Relationship between the empty DOS and the ELNES intensity in the ionization edge fine structure. Note the equivalence between the Fermi energy E_F and the ionization edge onset E_C. Electrons ejected from the inner shells reside preferentially in regions of the DOS that have the greatest density of unfilled states. The filled states below E_F are drawn as a quadratic function, but this is an approximation.

We discuss this fingerprinting approach in Section 40.2.D below and you can check it in the EELS Atlas or at URL #1. Remember, we did exactly the same type of fingerprinting of different phases with the low-loss spectra in Section 38.3.A.

40.2.B White Lines

Perhaps the most startling example of ELNES is the presence of the white lines, which we first saw in Chapter 39; these lines are intense sharp peaks on certain ionization edges. These sharp peaks arise because in certain elements the core electrons are excited into well-defined empty states, not a broad continuum, as in Figure 40.3. The $L_{2,3}$ edges of the transition metals and the $M_{4,5}$ edges of the rare-earth elements show such lines. The white lines in the Fe L edge are the L_3 and L_2 edges, respectively, as shown in Figure 40.4, and these specific lines arise because the d shell has unfilled states. (We'll explain what happened to L_1 later.) To explain these lines we need a little more quantum physics, which you can skip if you wish and go to the last paragraph of this section. You should also be aware that there is disagreement as to whether white lines are truly fine structure or strictly ionization edge (atomic) intensity; but we'll leave this somewhat arcane discussion to those who know better (another cause of fracas in bars at M&M meetings).
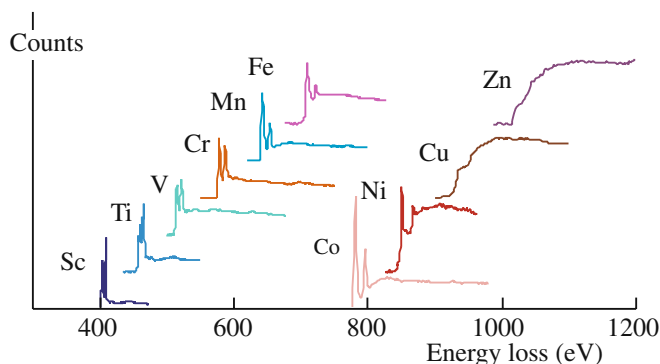
FIGURE 40.4. Spectra from the transition metals show a variation in the L_3 and L_2 white-line intensity ratios reflecting the variation in the number of core L-shell electrons ejected into unfilled d states. Note that Cu and Zn show no white lines because their d shells are full. The L_3 and L_2 white lines in the Fe L edge are the only ones that show the expected L_3:L_2 of ~2:1.

40.2.C Quantum Aspects

First, remember that the various electron energy levels, K, L, M, etc., correspond to principal quantum numbers (n) equal to 1, 2, 3, etc. Within those energy levels, the electrons may have s, p, d, or f states, for which the angular-momentum quantum number (l) equals 0, 1, 2, 3, respectively. The notation s, p, d, f comes from the original description of the atomic-spectral lines arising from these electron states, namely, sharp, principal, diffuse, and fine, although these terms have no counterpart in the EELS spectra we obtain.

As we noted in Section 39.1, the nomenclature $L_{2,3}$ arises from the fact that the L shell, from which the electron was ejected, has different energy levels. Such separation of the energies of the core states is called *spin-orbit splitting*.

Because the L electrons in levels 2 and 3 are in the p state, quantum theory demands that the sum (j) of their spin quantum number (s) and angular-momentum quantum numbers (l) is governed by the Pauli exclusion principle such that $j (= s + l)$ can only be equal to 1/2, 3/2, 5/2, etc. The spin quantum number, s (not to be confused with the s state), can only equal $\pm 1/2$. Taking all this into account, along with other quantum-number restrictions, it turns out that in the higher energy (i.e., more tightly bound) L_2 shell, we can have two p electrons with $j = \pm 1/2$ while in the L_3 shell, we can have four p electrons with $j = \pm 1/2, \pm 3/2$. Therefore, we might expect twice as many electrons to be excited from the L_3 shell as from the L_2 shell giving an L_3/L_2 intensity ratio (above the edge intensity, not above background) of 2. While this rule is approximately obeyed in the Fe spectrum shown in Figure 40.4, in practice, the ratio is seen to increase along the transition metal series from 0.8 for Ti to 3 for Ni, as is also seen in the spectral sequence in Figure 40.4.

Now these p-state electrons in the L shell cannot be excited to just any unoccupied state.

So for the p state ($l = 1$) the only permitted final states are either an s state ($l = 0$) or a d state ($l = 2$). Consequently, the core electrons are ejected primarily into the unoccupied d states in the conduction band, since there are few available s states there.

It is because of the dipole-selection rule that we don't see a strong L_1 edge in the spectrum. The L_1 edge sits closer to the nucleus than the L_2 and L_3 edges and its electrons are in the s state ($l = 0$) so they can only be excited to a p state ($l = 1$), but not to a d state ($l = 2$), or to another s state. Since there are few unfilled p states in

the conduction band of transition metals and they are much more spread out in energy than the d states, the L_1 intensity is very low and the peak is broad and may even be invisible in the $L_{2,3}$ post-edge structure.

(A)

(B)
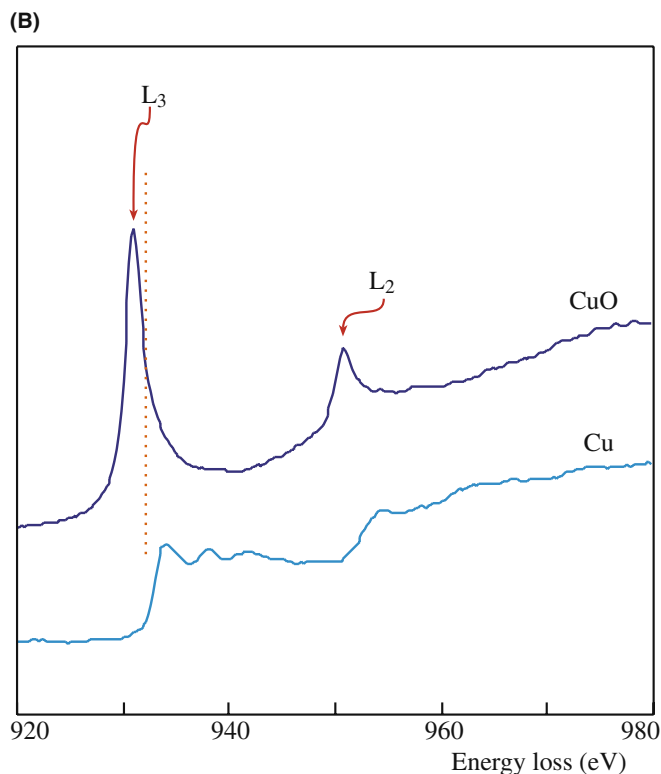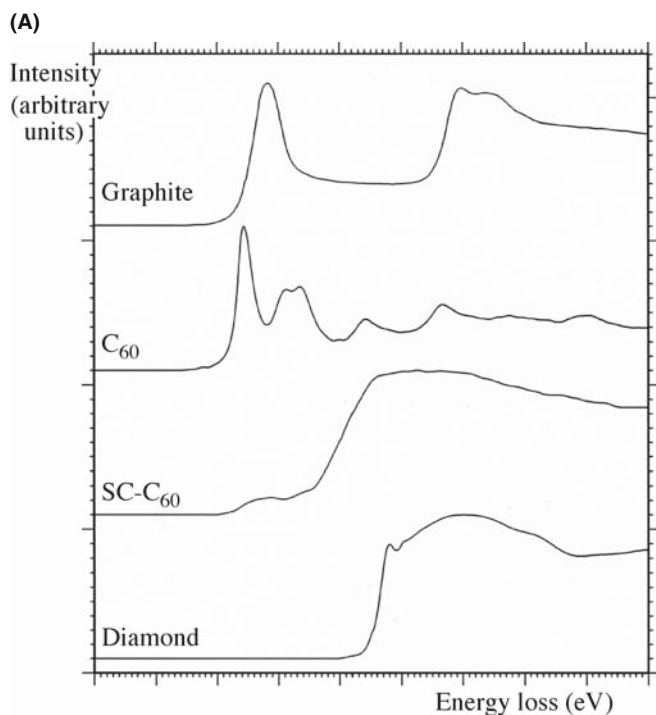
FIGURE 40.5. (A) Differences between the ELNES of the carbon-K edge from various forms of carbon. (B) Change in the Cu $L_{2,3}$ edge ELNES as Cu metal is oxidized and the filled d states lose electrons, thus permitting the appearance of white lines.

The energy width of the white lines is also affected by the time it takes for the ionized state to decay. One form of Heisenberg's uncertainty principle states that $\Delta E \Delta t = h/4\pi$, so a rapid decay gives a wide peak. For example, the Fe L_2 ionization can be rapidly compensated by an electron from the L_3 shell filling the hole and ejecting an Auger electron from the d shell. (This is called a Coster-Kronig transition.) A conduction band electron could also fill the L_2 core hole but the L_3 core hole can *only* be filled from the conduction band. Therefore, because there are two possible ways to fill the L_2 core hole, the L_2 line has a shorter Δt and a larger E than the L_3 line, which is much sharper.

In elements that don't have strong white lines, the ELNES is still present but appears just as weaker oscillations in intensity, which still reflect the DOS, and which, like the white lines, we can calculate and predict (much more of this later) (e.g., look at the pure-Cu ELNES in Figure 40.5C compared with the Fe ELNES in Figure 40.4).

40.3 APPLICATIONS OF ELNES

So let's see how all of this physics can be useful. (Is this an oxymoron?) The ELNES has been found to be dependent on details of the local atomic environment, such as coordination, valence state, and the type of bonding. Measurement of the fine structure, understanding how it is related to the electronic structure and ultimately to materials properties, can answer some hitherto-unsolved problems, particularly those where changes in bonding occur over small distances in your specimen. If you look at Figure 40.5, you'll see the carbon K edges for graphite and diamond. The carbon atom has hybridized s and p orbitals (termed σ and π in molecular-orbital theory). Graphite contains sp2 bonds in the basal plane with Van der Waals bonding between the planes. In contrast, the diamond structure has four directional, hybridized, sp3 covalent bonds and the atoms are tetrahedrally coordinated rather than arranged in graphitic sheets. The strong peak K edge at 284 eV identifies the empty π* states into which the K shell electrons are transferred in graphite, while the diamond K edge has no π* peak but shows a strong σ* peak at about 290 eV. This kind of information is also extremely useful in the study of thin diamond and diamond-like carbon films, which are of great interest to both semiconductor manufacturers and the coatings industry (sunglasses in particular). Carbon films can be made with a continuous range of graphitic and diamond-like character and it is possible to deduce the relative fraction of sp3 (diamond) and sp2 (graphite) bonding from the K edge ELNES (Bruley et al.). In today's world of carbon nanotubes, buckyballs, and graphene, all these newer forms of carbon can easily be

distinguished by their ELNES. For example, carbon K-edge spectra from C_{60} (Buckminsterfullerene of Bucky-balls) are also shown in Figure 40.5 in the standard and shock-compressed form. Another useful example is given in Figure 40.5B, where the changes in the Cu $L_{2,3}$ edge with oxidation are shown. This is a classic example. Since Cu metal has all its 3d states filled, there are no white lines in spectra from the metal. Upon oxidation, some 3d electrons are transferred to the oxygen, leaving unfilled states, and the white lines appear in the oxide spectrum. Note also that the onset of the oxide edge is different from that of the metal, because this electron transfer changes the value of E_C.

ELNES changes often occur at interfaces where the bonding changes locally over less than 1 nm. In Figure 40.6 the Si-K edge ELNES is seen to change across a Si-SiO$_2$ interface because the Si bonding changes. In this example, you can see the extraordinary power of an FEG STEM to provide simultaneous atomic-level images and spectra localized to individual atomic columns (even though this work (from Batson) is now more than 15 years old). The combination of Z-contrast imaging (see Section 22.4) and PEELS is arguably the most powerful analytical technique for atomic characterization, as we showed in Figures 39.22 and 39.23.
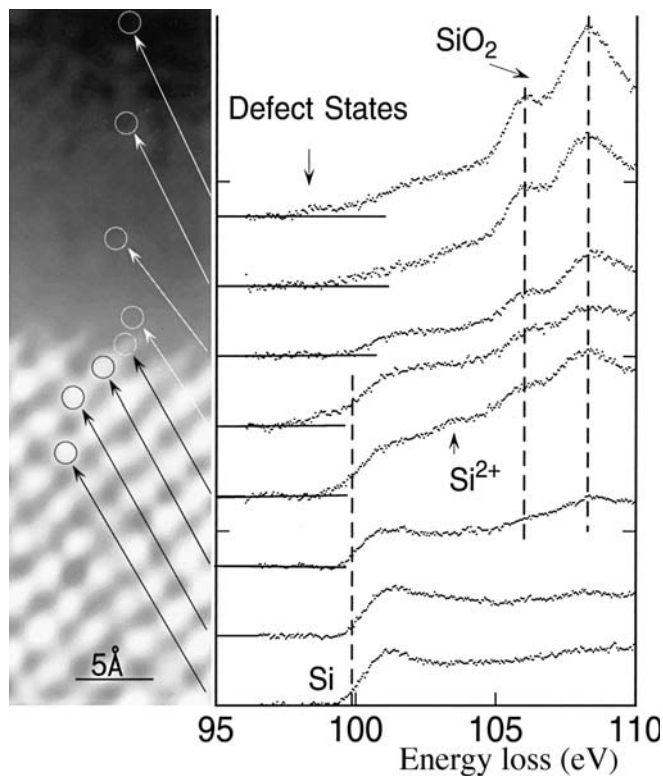
Bonding may also be changed by local segregation and one of the more powerful examples of ELNES is the detection of bonding changes associated with elemental segregation to interfaces, which can cause extraordinary changes in the mechanical properties of metals and alloys. For example, Ni$_3$Al has great potential as a high-temperature intermetallic, but is limited by its inherent brittle behavior resulting in intergranular fracture. It has been known for many years that this brittle behavior can be countered by the addition of a fraction of a percent of B which is known to segregate to the boundaries. Why this segregation results in a major ductility improvement was unknown until it was shown that, at B-containing boundaries, the Ni $L_{2,3}$ edge exhibits slight ELNES changes consistent with the more metallic-like bonding of pure Ni (see Muller et al.). In a complementary study, Keast et al. measured Bi segregation to Cu grain boundaries, and observed ELNES changes in the Cu $L_{2,3}$ edge, consistent with the Cu atoms in the boundary taking on a less-metallic bonding state (see Figure 40.7). This ELNES change, which is equivalent to the transfer of less than 0.3 electrons (whatever that means) from each Cu atom at the boundary to an adjacent Bi atom, may account for the brittle behavior of Cu doped with as little as 20 ppm Bi; an extraordinary change in mechanical behavior, noted first in 1874. Understanding the role of slight electronic bonding effects in such macroscopic behavior as brittle behavior may help to transform the power-generation industry for example, which spends billions of dollars removing impurity elements that cause catastrophic failure of pressure vessels if left to segregate to grain boundaries.

Such studies of ELNES are probably the most widely used aspects of EELS and the literature abounds with ELNES studies of valency determination and atomic coordination. Some examples include bonding changes at oxide interfaces on Si (Botton et al.) and probing the structure of potential next-generation Hf-based gate oxides in Si semiconductors (McComb et al.). Reviews of the potential and practical applications of ELNES have been given by Keast et al. and Brydson et al.

FIGURE 40.6. The change in the ELNES of the Si L edge across an interface between crystalline Si and amorphous SiO$_2$. Local electronic changes at the atomic level are easily discerned.
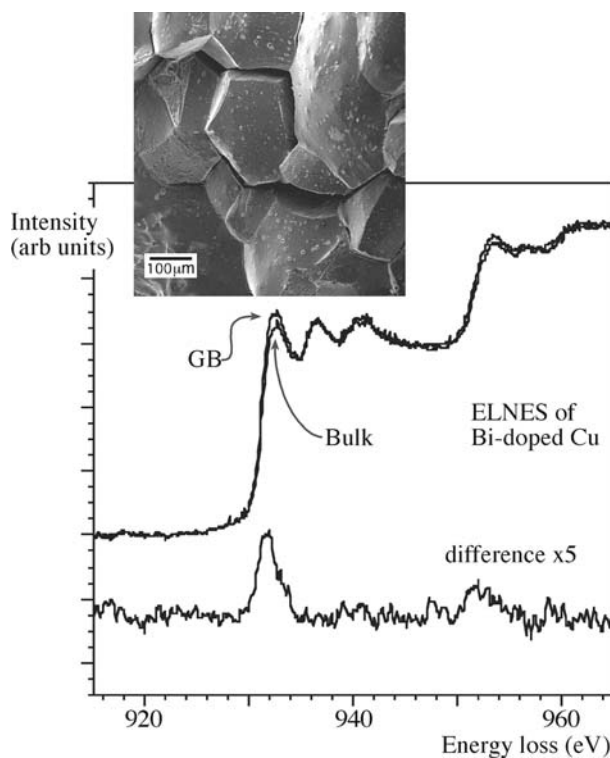
40.4 ELNES FINGERPRINTING

Although the ELNES is directly related to the details of the electronic structure, interpretation of particular features in an experimental spectrum is not always

FINE STRUCTURE AND FINER DETAILS
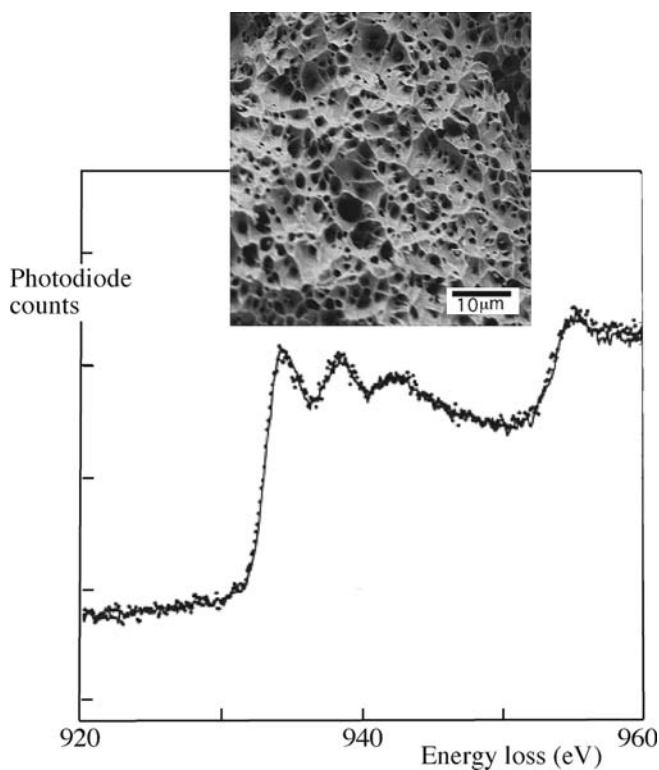
FIGURE 40.7. Change in ELNES due to impurity segregation. (A) Cu L$_{2,3}$ ELNES in pure Cu. (B) Slight Cu L$_{2,3}$ ELNES change between the bulk (grain interior) and a grain boundary to which Bi is segregated. The effect is magnified 5× in the difference plot. The two SE images show the extraordinary change in fracture behavior of ductile, pure Cu and brittle, Bi-doped Cu.

straightforward and you may not have the capability to carry out the atomic-structure calculations that we'll describe below. If this is the case, don't despair because you can still use a fingerprinting approach without fully knowing the details of the electronic structure. The idea behind such fingerprinting, as we've seen for the low-loss spectra, is that the general form of the ELNES is predominantly sensitive to the nearest-neighbor coordination and so it changes with changes in the structure. An example is provided by the Al-L$_{2,3}$ ELNES and Al-K ELNES of aluminum-oxygen materials which are sensitive to the local coordination of Al (i.e., whether octahedral or tetrahedral). Likewise, Figure 40.8 shows the experimental Mn-L$_{2,3}$ ELNES for different minerals in which the valence state of the Mn varies from 2+ to 4+. Again, we use the word fingerprint to emphasize that it is not necessary to understand the details of the DOS of complex materials in order to be able to interpret the ELNES spectra. Direct comparison with spectra from known standards is often all that is required for probable identification of the bonding state of a specific atom in your specimen. But because the matches are rarely perfect (given all the experimental and specimen variables that may affect the detailed intensity in the fine structure) go back and read our caution about low-loss

fingerprinting in Section 38.3.A and apply it to your ELNES fingerprinting. Note that you don't need the very best energy resolution to carry out fingerprinting: the data in Figure 40.8 were taken many years ago from a standard PEELS system and, for many cases, a LaB$_6$ source is fine.

A theoretical calculation of the unoccupied DOS will always be useful in understanding or predicting features in the ELNES. In the next section, we'll show some examples where modeling the ELNES has helped our interpretation.

40.5 ELNES CALCULATIONS

Many attempts have been made to compare the experimental ELNES with calculations of the DOS in simple materials, such as metals and oxides. Great strides have been made in the last few years, mainly in improvements in models of the atomic potentials and in the computing power needed to pursue the calculations. This aspect is transforming the study of ELNES from an esoteric field to one with broad applications in materials science. This topic is also addressed in substantial depth in the companion text.
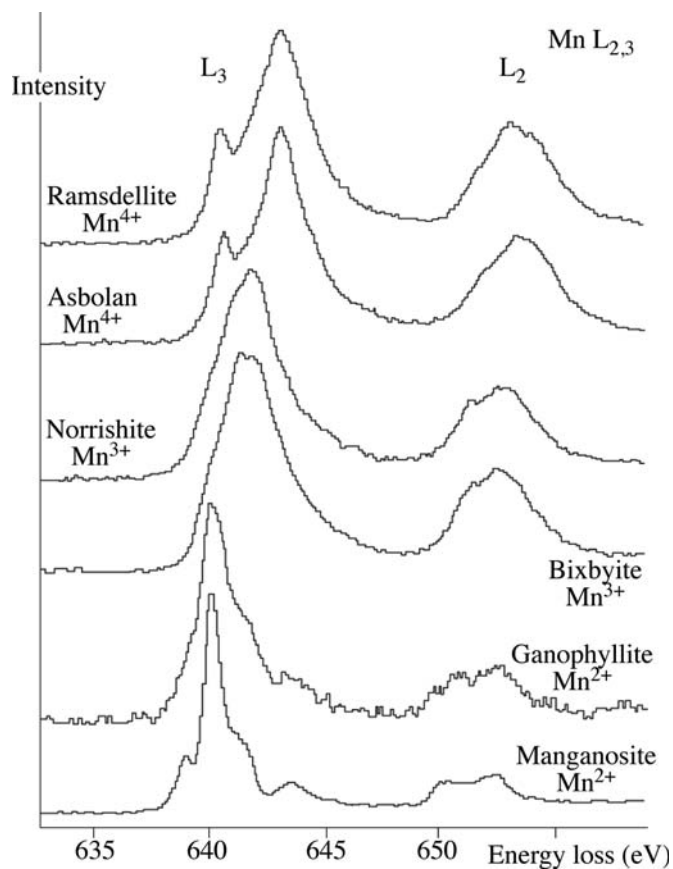
FIGURE 40.8. Comparison of Mn L$_{2,3}$ ELNES from a range of minerals in which the Mn coordination and hence valence state changes. The L$_2$ and L$_3$ white lines broaden as the oxidation state increases from +2 to +4 and in some cases the L$_3$ peak splits into two peaks. Understanding why such changes happen from an electronic standpoint is not necessary for identifying the different minerals or valence states.

40.5.A The Potential Choice

Calculating the electronic structure in solids involves solving the Schrödinger equation for each electron in the potential of the solid, including the Coulomb potential of both the nuclei and all the other electrons. (Now might be a good time to move on to the next section if you haven't recognized too many words in the previous sentence!) We also have to include terms due to the fact that the electrons are affected by the presence of other electrons and their behavior is correlated (i.e., they aren't isolated particles). Given the large number of electrons involved in any calculation, we often use an approach called density-functional theory (DFT) (if you're into physics and want to go to the next level (or two) then you need to read Finnis' (2003) book on atomic-modeling which includes DFT). Out of DFT comes a simplifying assumption, which we call the local-density approximation (LDA). Within the LDA method, we choose one of three different approaches to perform our calculations, which basically come down to a choice of atomic potential

- We can calculate the band structure directly in reciprocal space. This is usually described as the band-theory approach and the electron states are formed in a repeating crystal lattice. If this reminds you of Bloch states, back in Chapter 14, you're right.
- We can describe the electron states in terms of molecular orbitals (MO).
- We can calculate the effect of multiple scattering (MS) of the electron wave in real space based on the model shown in Figure 40.1A.

A range of band-structure methods are used and they go by rather strange names, such as augmented plane wave (APW), full-potential linearized APW (FLAPW) (URL #2), augmented spherical wave (ASW) (URL #3), CASTEP (URL #4), Layer Korringa-Kohn-Rostoker (LKKR), pseudopotentials, and other methods. The URLs will lead you to the sites for the various public-domain or commercial versions of the software. The best name by far is the muffin-tin (MT) potential (URL #5), which is spherically symmetric at the atomic positions and flat between them. (Apparently, to some physicists, this shape looks like a cross section of a tin used to bake muffins.) This model modifies the classic energy diagram, as shown in Figure 40.9. The MT form is useful because it generates wave functions that we can break down into the various angular-momentum components (which describe the partial DOS which is reflected in the ELNES). However, most MT approaches assume the crystal lattice is infinite and you need Bloch's theorem for the wave-function calculations which give the DOS. You'll probably find these techniques computationally challenging and not very flexible. But with the advent of easily available, high-performance, parallel computing, we are no longer so constrained (see the next section). For example, only recently have MO theorists been able model large unit cells, planar interfaces, and those (now-ubiquitous) amorphous materials.

THE TERMINOLOGY

Pseudopotential
MT: Muffin-tin potential
DOS: density of states
DFT: density functional theory
LDA: local density approximation
APW: the augmented plane wave
FLAPW: the full-potential linearized APW

MO theory is just an extension of using molecular orbitals to describe solids. (Not surprisingly, this approach is often used by chemists!) To use this approach, we have to divide our specimen into separate molecular units. If we calculate the MOs for each unit,
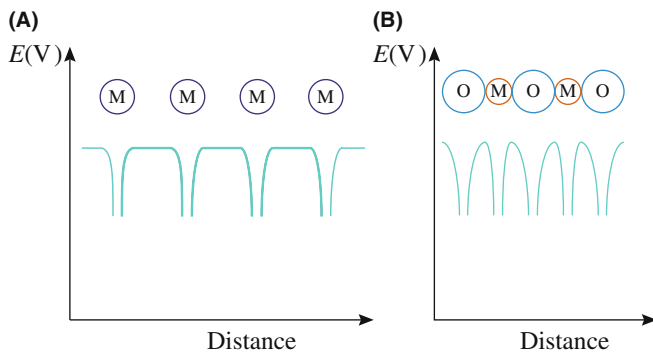
FIGURE 40.9. The muffin-tin potential energy diagram for (A) a metal and (B) an oxide. Note the symmetry of the potential wells for the metal and the asymmetry for the oxide.

we can then interpret the ELNES spectra in terms of core-shell electrons being ejected into unoccupied MOs. These unoccupied MOs arise because the excited-atom orbitals interact (i.e., bond) with nearest-neighbor atoms. (This is the π/π* and σ/σ* bonding/antibonding orbital notation that we used to describe the C-K shell ELNES back in Figure 40.5A). We can extend this idea and imagine the various MOs as simply linear combinations of atomic orbitals (which is then called the LCAO approach). LCAO works well if the orbitals are occupied but, for unoccupied orbitals, we have to use the self-consistent field (SCF) method, which basically assumes that the atoms are organized in a localized molecular cluster which then uses a version of the MS method which we'll now describe.

MS (not Word!) calculations are based on the interpretation of the ELNES as scattering of the electron wave that emerges from the ionized atom by atomic shells around that excited atom (which we started with back in Figure 40.1). Still the most elegant MS method is that due to Durham et al. The Durham method first divides the cluster of atoms into shells, each approximately equidistant from the ionized atom. We then solve the scattering within each atomic shell in turn. Finally, we consider scattering between different atomic shells. Since we have to calculate *all* possible scattering paths it's much easier in crystals because we can use their symmetry to facilitate our calculations. A self-consistent version of the MS method called FEFF (now in version 8) is commercially available (URL #6) and highly recommended. You can extend this shell-by-shell MS approach to model much more complex amorphous systems, incommensurate structures, and non-periodic atomic arrangements at planar interfaces and defects. You'll find that the MS calculations predict modulations in the near-edge intensity, which correspond directly to the DOS of the ionized atom. So you should be aware that these calculations are only an *interpretation* of what actually happens to the electron after it emerges above the Fermi level. Also, many

calculations of ELNES only show reasonable agreement with experiment when the effect of the core hole is included, so we now need to explain this terminology.

Figure 40.10 gives a comparison of the experimental C-K edge ELNES from TiC with the results of calculations using several different potentials, none of which reproduce the experimental spectrum precisely but all of which capture some aspects of the general shape.

40.5.B Core Holes and Excitons

Having chosen an atomic potential, we actually determine the ELNES (using the MS approach) by calculating all possible inter- and intra-shell scattering events suffered by the electron after it emerges above the Fermi level. One of the problems that confuses this issue is that the ionization event results in a hole in the core shell which, of course, changes the atomic potential.

A bit more physics: The ionization process occurs in the time taken for the beam electron to traverse the diameter of the particular inner shell. We know that a 200-keV electron has a velocity, $v = 2.7 \times 10^8 \, ms^{-1}$, and the K-shell of oxygen, for example, has a diameter of ~0.01 nm, so the ionization process occurs over ~10^{-19}–10^{-20} s. By comparison, the atom stays in its excited state (which is a
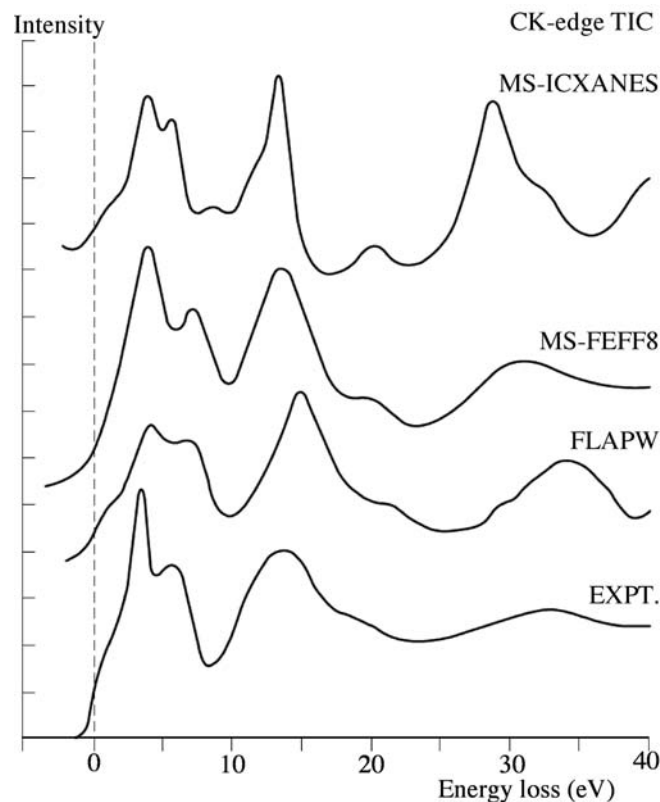
FIGURE 40.10. Comparison of the experimental C K-ELNES from TiC (*Expt.*) with the results of theoretical modeling calculations using both a band-structure code (*FLAPW*), and two different MS codes (*FEFF8* and *ICXANES*).

combination of the lifetimes of the excited electron and the lifetime of the hole in the inner-shell) for much longer, because the hole decays in $\sim 10^{-14}$–10^{-15} s. Because the lifetime of a hole is $10^5 \times$ longer than the excitation process, the outermost electron states, including the final state of the excitation process, will experience an attractive potential because of the core hole, which behaves like an extra nuclear charge on the atom. So, in fact, all we do to compensate for this is assume that the ionized atom now has a nuclear charge of $Z+1$, rather than Z, because the missing electron lowers the shielding affect of the core electrons. This extra positive charge may be shielded by other electrons (e.g., weakly bound valence electrons) which will move in response to the existence of the hole and reduce its effect. Despite this screening (go back and check Section 3.5 to remind yourself what this term means), the core-hole potential will tend to attract the outer electron states more strongly. So the available final states for the ejected electron, in the presence of the long-lived hole, will tend to be more sensitive to the short-range environment of the excited atom and, of course, this will be reflected in the ELNES.

40.5.C Comparison of ELNES Calculations and Experiments

The 1982 seminal paper in the field of ELNES experiments on transition metals and oxides is by Leapman et al. For further examples, you should read the review articles which we mentioned at the end of Section 40.3. We'll just show a couple of examples here but the literature contains many. The difference due to different coordinations is obvious. The sharp peak at the Al L edge onset is thought to be an exciton. This effect is not well modeled by the theory, which otherwise makes a good match with the experimental data.

The electron energy-loss near-edge structure (ELNES) at the O K edge has been studied in yttria-stabilized zirconia (YSZ) (Ostanin et al.). The electronic structure of YSZ for compositions between 3 and 15 mol.% Y_2O_3 has been computed using a pseudopotential-based technique to calculate the local relaxations near the O vacancies. The results showed phase transition from the tetragonal to cubic YSZ at 10 mol.% of Y_2O_3, reproducing experimental observations. Using the relaxed defect geometry, calculation of the ELNES was carried out using the full-potential linear muffin-tin

orbital method. The results show very good agreement with the experimental O K-edge signal, demonstrating the power of using ELNES to probe the stabilization mechanism in doped metal oxides.

If an atom exists in two different environments in a structure, then we can make the approximation that the ELNES is simply a linear superposition of the contributions from the two environments and experiments tend to support this simple approach.

It's perhaps best to conclude with the conclusion of Duscher et al.

"We have reached a level of agreement between theory and experiment not achieved previously in such a range of different materials by including a localized core-hole effect. There was no significant difference between both the methods used, a core hole in an all-electron method and the $Z+1$ approximation. This approach is sufficiently robust to proceed to interface structures."

In other words, theoretical calculations are a well-established and useful field of ELNES research and this is explored much further in the companion text. One last and obvious point to note is that, because the ELNES signals are often quite strong, it is straightforward to map out different portions of the ELNES, thus imaging, in effect, changes in the DOS and localized variations in atomic bonding, with the usual high resolution expected of EFTEM images. An example is shown in Figure 40.11.

40.6 CHEMICAL SHIFTS IN THE EDGE ONSET

We can think of the atoms in our specimen as having different charges with respect to one another (which we otherwise call electronegativity). So any changes in the charge in different systems will lead to changes in the binding energies of the various (occupied and unoccupied) electron states and it's reasonable to ask if we could detect this binding-energy change in EELS. We already know that (for a hypothetical, single, isolated, hydrogen atom) the ionization-edge threshold energy is effectively the critical ionization energy, E_C. However, in a real material, the experimental-edge onset corresponds to the difference in energy between the initial state and the lowest unoccupied final state *in the presence of the core-hole*. More often than not, it is extremely difficult to determine accurately the threshold energy, which often lies above the experimental-edge onset. Changes in the effective charge on the atom affect the energies of both the initial and final states. Unlike the deep-lying core orbitals, the outer orbitals are easily influenced by factors, such as bonding. If we consider changing from a metal to an insulator, the presence of a band gap in the insulator will result in a shift of the edge
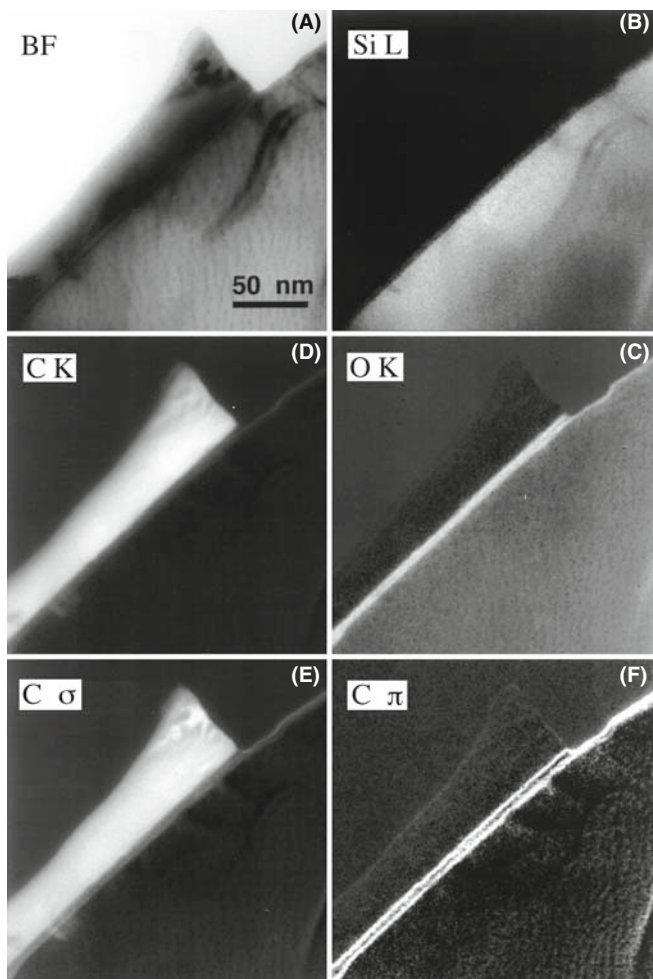
FIGURE 40.11. (A) TEM BF and (B–F) a series of energy-filtered images revealing the Si, C, and O elemental distributions and the carbon bonding maps at the interface between a diamond-like carbon film and a Si substrate. In the oxygen-rich amorphous layer at the interface, there is a double layer of carbon atoms that is primarily π-bonded (and possibly arises from carbon contamination in surface grooves at the interface) (F). The carbon film is predominantly σ-bonded (E), indicating a high degree of diamond-like character.

onset to higher energy loss. For example, the $Al-L_{23}$ edge shifts from 73 eV in the metal to 77 eV in Al_2O_3, and we saw similar behavior for the Cu/CuO spectra in Figure 40.5B. Another example is provided by the C-K edges in Figure 40.5A, in which shifts in the π^* peak position are easier to see than changes in the rather ill-defined edge onsets.

Similar edge-onset shifts are well known in XPS and are called chemical shifts. They are reasonably well understood and we can often predict them theoretically. However, the electron-excitation process in EELS is more complicated than X-ray induced ionization (detected in XPS), particularly the unavoidable presence of the core hole and the variable extent to which it is screened by the remaining electrons. Consequently, in comparison with X-rays, little systematic work on EELS chemical shifts has been done, apart from fingerprinting experimental

spectra and comparing them with reference materials. While we can correlate the edge-onset energies with such variables as oxidation states, atomic charge, and coordination, there is room for considerable improvement in calculation of the true edge-onset energies. It's worth noting that the possibility of a chemical shift in the edge may make it difficult to interpret ELNES intensity changes detected by difference techniques (such as the example shown back in Figure 40.7B). However, careful experimentation should minimize this danger.
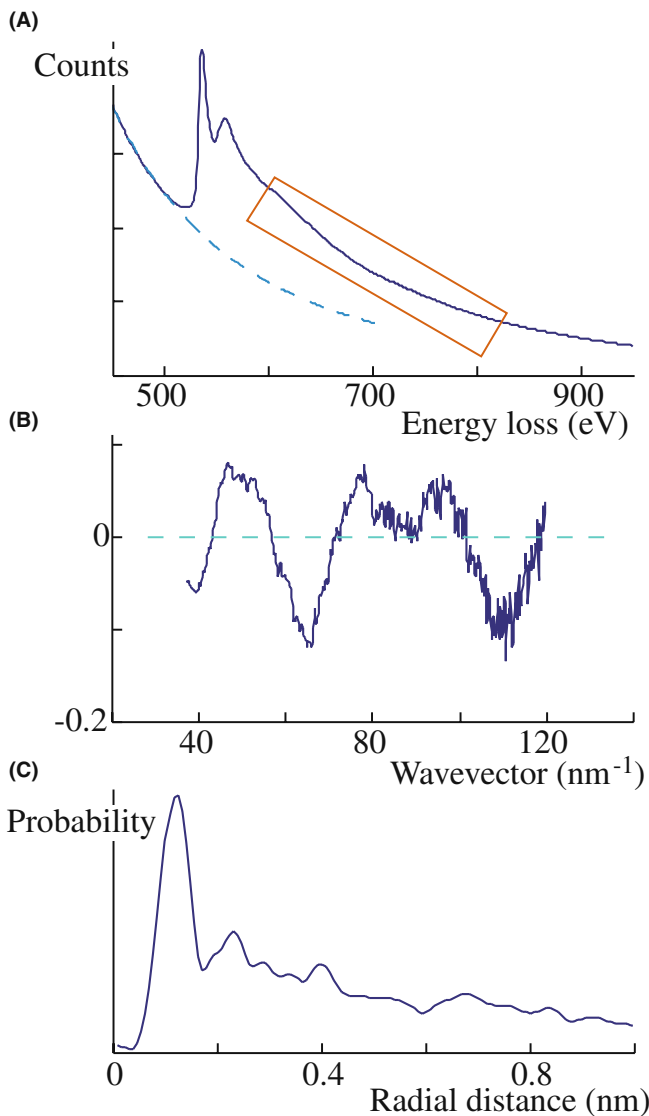
40.7 EXELFS

If, after an atom is ionized, the ejected electron does not fill an empty state but escapes outside the atom, then it acts like a free electron (typically with energy >50 eV). We can interpret this excess energy as an electron wave, which can be diffracted by the atoms in the structure around the original ionization site. Because the electron has higher energy than those which gave rise to multiple-scattering ELNES, the diffraction is assumed to be a single-scattering event, as shown back in Figure 40.1B, and this diffraction causes oscillations on the otherwise smooth DOS. We call these oscillations extended energy-loss fine structure or EXELFS. As with any diffraction event, there is information in these EXELFS ripples about atomic positions and the atomic information comes from a relatively short range (the first few nearest neighbors) since this weak electron doesn't scatter from more distant atoms.

> **ELNES AND EXELFS II**
> ELNES is multiple scattering and EXELFS is single scattering, although the two phenomena overlap since, e.g., the L_1 ELNES peak is often far enough past the edge onset to be included in the EXELFS.

The EXELFS modulations start about 50 eV above the ionization-edge energy, are each 20–50 eV wide, as shown in Figure 40.12A, and occur over several hundred eV. EXELFS is closely analogous to the oscillations seen in the extended X-ray absorption (edge) fine structure (EXAFS) in synchrotron X-ray spectra and is one reason why EELS has long been described as a synchrotron in a TEM (albeit much cheaper than your typical synchrotron). One significant difference is that EXAFS results in complete photoabsorption of the incident X-ray while EXELFS involves absorption of only a small fraction of the energy of the beam electron. We can carry this analogy a little further. Both EXAFS and EXELFS give us structural information from materials in which there are strong, local, atomic correlations. Both techniques are atom specific so, in principle, we can solve even the most complex multi-component

(A)

Counts

500   700   900
Energy loss (eV)

(B)

0

-0.2
40   80   120
Wavevector (nm^{-1})

(C)

Probability

0   0.4   0.8
Radial distance (nm)

FIGURE 40.12. (A) EXELFS modulations on an ionization edge. (B) From the oscillations in the post-edge spectrum it is necessary to transfer the data to k-space before (C) Fourier transforming the data to produce a radial-distribution function.

structures, if the information around all the atoms can be accessed.

There are, however, limitations to conventional EXAFS.

- We can't easily access the K-edges below 3 keV since X-ray absorption at these low energies requires thin specimens for transmission-EXAFS and a low absorption atmosphere over the entire X-ray beam path (source-specimen-detector).
- As you know from the XEDS chapters, X-rays cannot easily be focused to a sub-micrometer spot, so EXAFS has a relatively low spatial resolution, although this is constantly improving. EXELFS offers us the unique ability to obtain atomic and

electronic structure with nanometer-scale spatial resolution.

- Since TEMs operate in high vacuum and use thin specimens, EELS is more naturally suited to K-edge analysis of low-Z elements (as well as L-edge analysis of higher-Z elements) than low-energy EXAFS.

There is the usual price to pay for high spatial resolution in that the EXELFS signal is noisy and you'll find that extracting high-quality atomic information is much more challenging than for EXAFS where there is no shortage of signal.

40.7.A RDF via EXELFS

With EXELFS we can determine the partial radial distribution function (RDF) around a specific atom, and we are not restricted to the heavier atoms ($Z>18$) needed for EXAFS. So there is great potential for studying materials, such as low-Z glasses, amorphous Si, bulk metallic glasses, and quasicrystalline structures (both of the latter two often contain relatively low-Z elements such as Be, Mg, Al, P). In particular, since glasses lack any long-range periodic structure, we are limited in the techniques to determine their atomic structure. As you've already seen back in Section 18.7, diffraction of electrons (or X-rays or neutrons) from glass provides only diffuse information. To get atomic-structure information from glasses, you have to employ resonance signals from the Å-level and EXELFS can do that. The high spatial resolution of EXELFS is obviously advantageous and all your data can be compared with your images and the rest of the TEM-based information that you acquire from the analyzed volume. However, you can't get good EXELFS unless your specimen is very thin and you'll also have to consider phase effects, which are averaged out in EXAFS. Despite these apparent advantages of EXELFS, RDF work continues to be dominated by synchrotron X-ray sources because of the intensity of the signal. If you're interested in pursuing this (and EXELFS for that matter), a good place to start is the text by Koningsberger and Prins.

DECONVOLUTION AGAIN
Deconvolution is always the first step if your specimen isn't thin enough, i.e., if the plasmon peak is greater than 10% of the ZLP.

Experimentally, it's not easy to see the EXELFS modulations because they are only ~5% of the edge intensity, and so you need good counting statistics. This is one of the rare cases where you might find a thermionic source useful because it can deliver more

total current than a FEG and, for this application, energy resolution is not so important. TEM diffraction mode will also increase your total signal intensity. Either way, however, you pay a price in terms of a loss of spatial resolution and an increased chance of specimen damage. If you need the best spatial resolution, a FEG STEM should (as usual) be your instrument of choice.

So, we're interested in EXELFS because of the structural information contained in the weak intensity oscillations. To extract this information, you can use the commercial Gatan software (see Section 1.6) or the EXELFS version of Rehr's FEFF code (URL #6). Public-domain EXELFS software is also available at URL #7.

You first have to ensure that your spectrum contains only single-scattering information, otherwise the plural-scattering intensity may mask the small EXELFS peaks. Deconvoluting the point-spread function may also help sharpen the faint modulations.

Next, you have to remove the background if it wasn't done prior to deconvolution. Then your spectrum intensity has to be converted to an electron-wave function in k-space (reciprocal space) where

$$k = \frac{2\pi}{\lambda} = \frac{[2m_0(E - E_K)]^{\frac{1}{2}}}{h} \tag{40.1}$$

where E_K is the edge onset energy, E is the energy of the ejected electron, of wavelength λ, and the rest of the terms have their usual meaning. The electron-wave interference gives periodic intensity maxima in k-space when

$$\left(\frac{2a}{\lambda}\right)2\pi + \Phi = 2\pi n \tag{40.2}$$

Here a is the distance from the ionized atom to the first scattering atom, and Φ is the phase shift that accompanies the scattering. Therefore, we expect to see periodic maxima occurring for $n = 1, 2$, etc., and for different interatomic spacings. We obtain the atomic spacing by Fourier transforming the k-space modulations to give the RDF, originating at the ionized atom. Obviously, these two equations don't tell the full story and there is more about data analysis in Egerton's book.

When we have the RDF, we ought to be able to determine the local atomic environment, if the various interferences can be discriminated and identified. Peaks in the RDF indicate the probability of an atom occurring a certain distance from the ionized-atom site. Figure 40.12 shows a summary of the EXELFS data extraction technique. Despite the low signal problems, EXELFS studies appeared at the earliest stages of EELS research (see, e.g., Leapman and Cosslett) and references to the technique have continued to surface in the

literature over the intervening decades. For example, Sikora et al. have compared EXELFS and EXAFS applied to crystalline materials. Alamgir et al. have made comparisons of the two techniques for the study of slow-cooled, bulk metallic glasses (a fascinating new range of materials). Figure 40.13 shows the extraction of EXELFS data from the P-K edge (inaccessible in a synchrotron spectrum) from Pd-Ni-P, a model amorphous metal. The various steps involve first the isolation of the fine structure (Figure 40.13A) and expressing it as a function of momentum transfer (k), $\chi(k)$, from beyond the P K-edge (Figure 40.13B). The Fourier transform of $\chi(k)$, FT[$\chi(k)$], is proportional to the partial radial distribution function of atoms around P (Figure 40.13C). Upon back-Fourier transformation of the first peak FT[$\chi(k)$], the contribution to $\chi(k)$ from the first coordination shell around P in these glasses is determined (Figure 40.13D). Similar exercises could be performed from the second and higher shells although the quality of the signal degrades rapidly. These data are then fitted with calculated $\chi(k)$ functions of various model structures using the multiple-scattering ab-initio code FEFF7 and a possible model of the coordination of Pd and Ni atoms around the P atoms is created.

40.7.B RDF via Energy-Filtered Diffraction

RDF data acquired through EXELFS complement another TEM method of acquiring RDF information. This involves energy filtering of SADPs by scanning the pattern across the entrance aperture to the PEELS using post-specimen scan coils. (See, e.g., McBride and Cockayne; see also Section 18.7.) Effectively, a full spectrum is available at each scattering angle, but, in fact, only the zero-loss (ideally only the elastic) electrons are required. The plot of the ZLP intensity as a function of scattering angle constitutes a line profile across a filtered DP from which the RDF can be extracted. This process does not have the spatial resolution of EXELFS, since typical SADPs are integrated over $\sim$0.2–1 μm^2, but the signal is much stronger. Accuracies of $\pm$0.001 nm in nearest-neighbor distances can be obtained, and the process is rapid enough to be performed on-line.

40.7.C A Final Thought Experiment

ELNES and EXELFS are really quite remarkable demonstrations of quantum theory and the wave-particle duality. Consider that the EXELFS part of the spectrum only contains electrons that have been scattered by electrons in the specimen atoms, and yet we are able to deduce information about what happened to those atoms *long after the beam-specimen interaction occurred* and also deduce where the scattering atom sits in the structure!
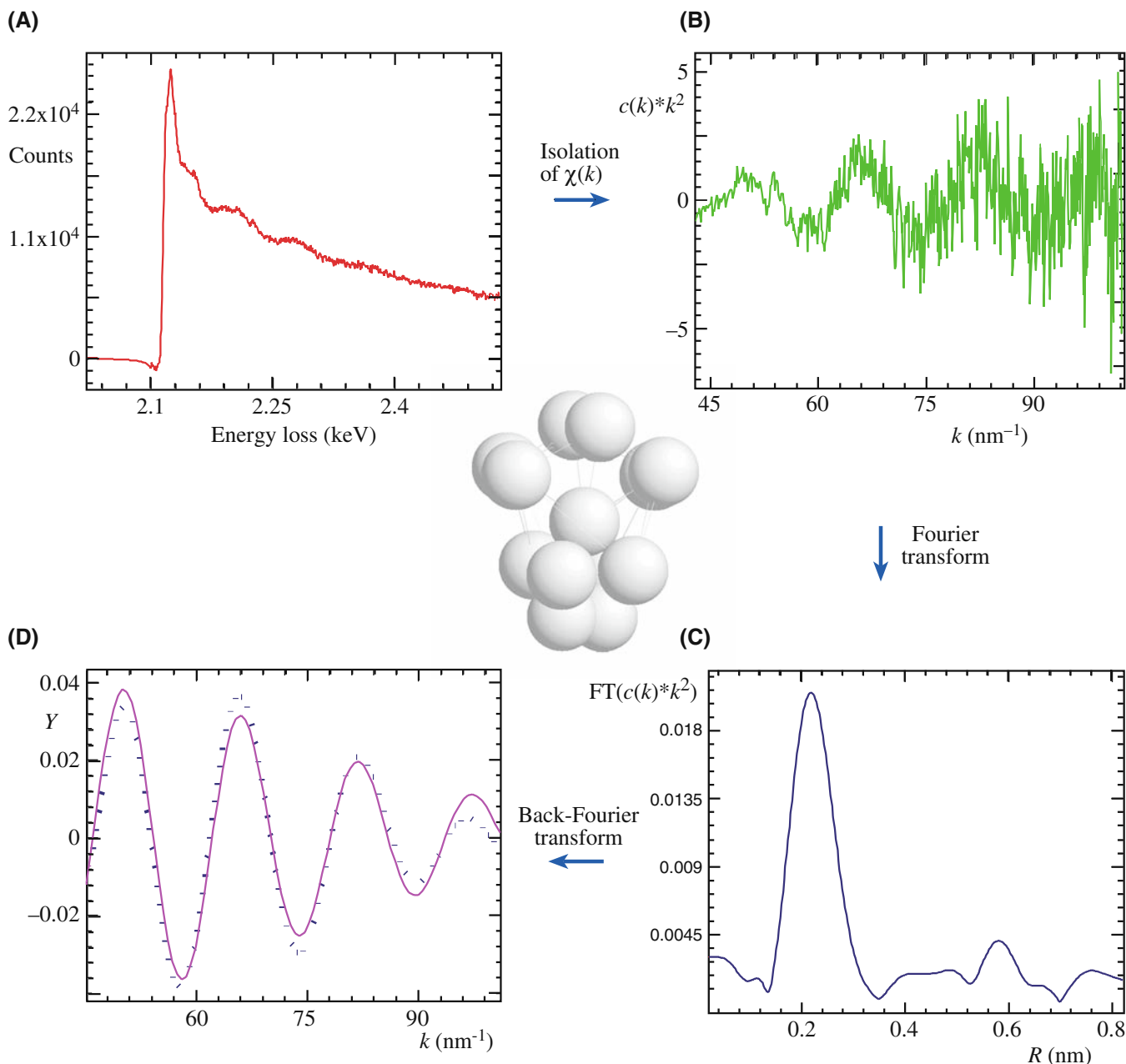
FIGURE 40.13. The EXELFS analysis of $Pd_{30}Ni_{50}P_{20}$ bulk metallic glass. (A) The pre-edge, background-subtracted P K-edge. (B) The isolated $\chi(k)$ data. (C) The Fourier transform of $\chi(k)$ to radial space, $FT[\chi(k)]$, and (D) the back-Fourier transform of the first peak of $FT[\chi(k)]$ back to k-space (dots) and fitting with a calculated function for a tetragonal dodecahedron (dashed line). The model in the center is a tetragonal dodecahedron with a P atom at the center surrounded by a first nearest-neighbor shell of Pd and Ni atoms deduced from the EXELFS.

An (approximately wrong) particle-based analogy would be to imagine that we are catching bowling balls that have been thrown at pins, arranged in a certain pattern. (Although instructive, this exercise is best carried out as a thought experiment.) From the velocity (energy) of the balls that we catch, we are able not only to identify the weight of the pin that was hit (i.e., identify the characteristic ionization edge), but we can also deduce how the pin fell down and where it rolled (the ELNES). Furthermore, we can also work out the spatial arrangement of the surrounding pins that didn't fall down (the EXELFS).

So how does the beam electron know where the core electron went after it left the inner shell? The answer lies in the fact that the bowling ball (particle) analogy is totally inadequate. In fact, only certain electron transitions are allowed and the beam electron can therefore only transfer certain quantized energies to the core electron, not a continuum of possible energies. So the beam electron does, in effect, 'know' the possible final state of the core electron since it reflects that state in its energy loss. (If you really understand this, then you should pat yourself on the back.)

40.8 ANGLE-RESOLVED EELS

Most of the time so far, we've been talking about gathering spectra and images by sending the direct beam into the spectrometer and splitting it up into its component energies. This is often called *spatially resolved* EELS since we map out a specific region or gather individual spectra from different spatial locations on the specimen. However, we have occasionally mentioned that the *angle* of scatter of the energy-loss electrons is important, and there is a whole field of EELS research that studies angle-resolved spectra. To do this, we just scan the DP across the PEELS entrance aperture and gather spectra at different angles as for the RDF measurements that we just described. However, rather than studying the energy of electrons primarily, this technique emphasizes the determination of the *momentum* of the energy-loss electrons. Momentum-transfer studies were pioneered by Silcox and co-workers. Now with FEG STEMs you can get even more information about the symmetry of electronic states, which complements spatially resolved ELNES (e.g., Wang et al.).

Because of such angular effects, the size of the spectrometer entrance aperture and/or the collection angle β may influence the details of ELNES. If the final state of the ejected electron has a definite directionality, as it will in an anisotropic crystal, the ELNES for such a specimen will depend on both the scattering angle θ and the crystal orientation. The classic paper on orientation or momentum dependence is the study of graphite and BN (Leapman et al.).

There are various ways of performing angle-resolved EELS and Botton and co-workers describe many methods and applications. For a given energy loss and a given specimen orientation, the momentum transfer at zero scattering angle, θ, is parallel to the electron beam ($q_{\parallel}$). As θ is increased, a component perpendicular to the beam is introduced ($q_{\perp}$) and, at approximately θ_E, $q_{\perp}$ becomes dominant. To obtain angle-resolved ELNES, we have to measure the spectra as a function of the angle between a crystal direction and the direction of momentum transfer.

First, you can keep the orientation fixed and change the collection aperture. Figure 40.14 shows angle-resolved ELNES of a very thin (∼ 30 nm) graphite flake obtained by changing the size of the collection aperture in a STEM. The π* states are parallel to the *c*-axis, which in this case is parallel to the electron beam. Therefore, the corresponding π* peak intensity is larger, relative to the σ* states, when we have a small collection aperture and $q_{\parallel}$ dominates. Similar effects would be obtained if the orientation of the graphite planes to the electron beam was changed.

Second, you can keep your collection angle fixed at a small angle $< \theta_E$ and measure the ELNES as a function of θ. This is particularly easy with energy filtering which can display angular scattering distributions of specific energy-loss electrons.
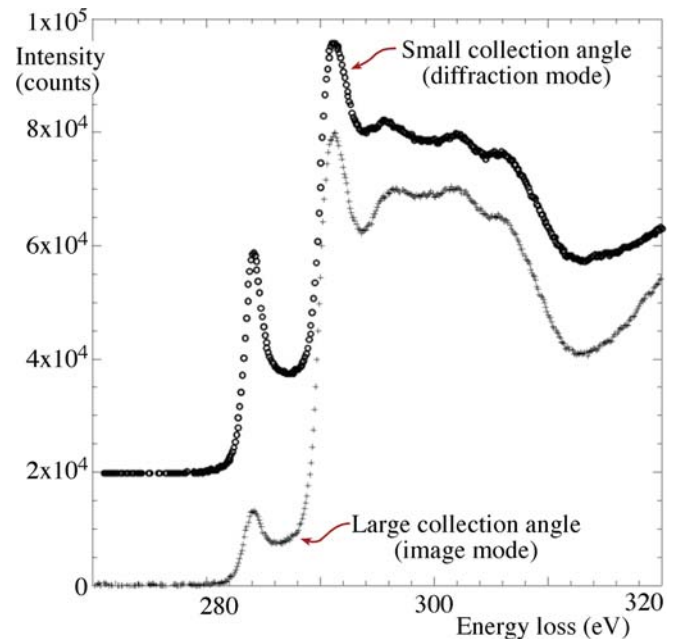
FIGURE 40.14. Image mode EEL spectra of the C-K edge in graphite showing changes in the relative intensities of the π* and σ* peaks under two different collection angles due to the directional scattering variation from the sp2 and sp3 bonds in the graphite.

You can also use the '45° method' (Botton) which combines tilting the specimen at 45° to the principal axis and measuring the ELNES at ±θ, where θ is chosen to select both $q_{\perp}$ and $q_{\parallel}$. If you make the beam convergent (e.g., in STEM mode for high spatial resolution) then the angular resolution of this technique is reduced.

One practical aspect of angle-resolved EELS is the study of Compton scattering, which is the ejection of outer-shell electrons by high-energy photons or electrons. We can detect these Compton-scattered electrons by observing the EELS spectrum at a high scattering angle (θ ∼100 mrad), either by displacing the objective aperture to select an off-axis portion of the diffraction pattern or by tilting the incident beam. This process has been used to analyze the angular and energy distribution of Compton-scattered electrons and determine bonding information, since the Compton-scattering process is influenced by the binding energy.

40.9 EELS TOMOGRAPHY

We've talked about tomography in various parts of the book and how taking a series of images at different tilts allows you to reconstruct 3D information about features within your specimen. You should also read the chapter in the companion text which gives an in-depth review of the various experimental challenges for this kind of imaging.

Just as for X-ray images, it is possible to use a full-tilt series of EFTEM images to build up a full 3D image
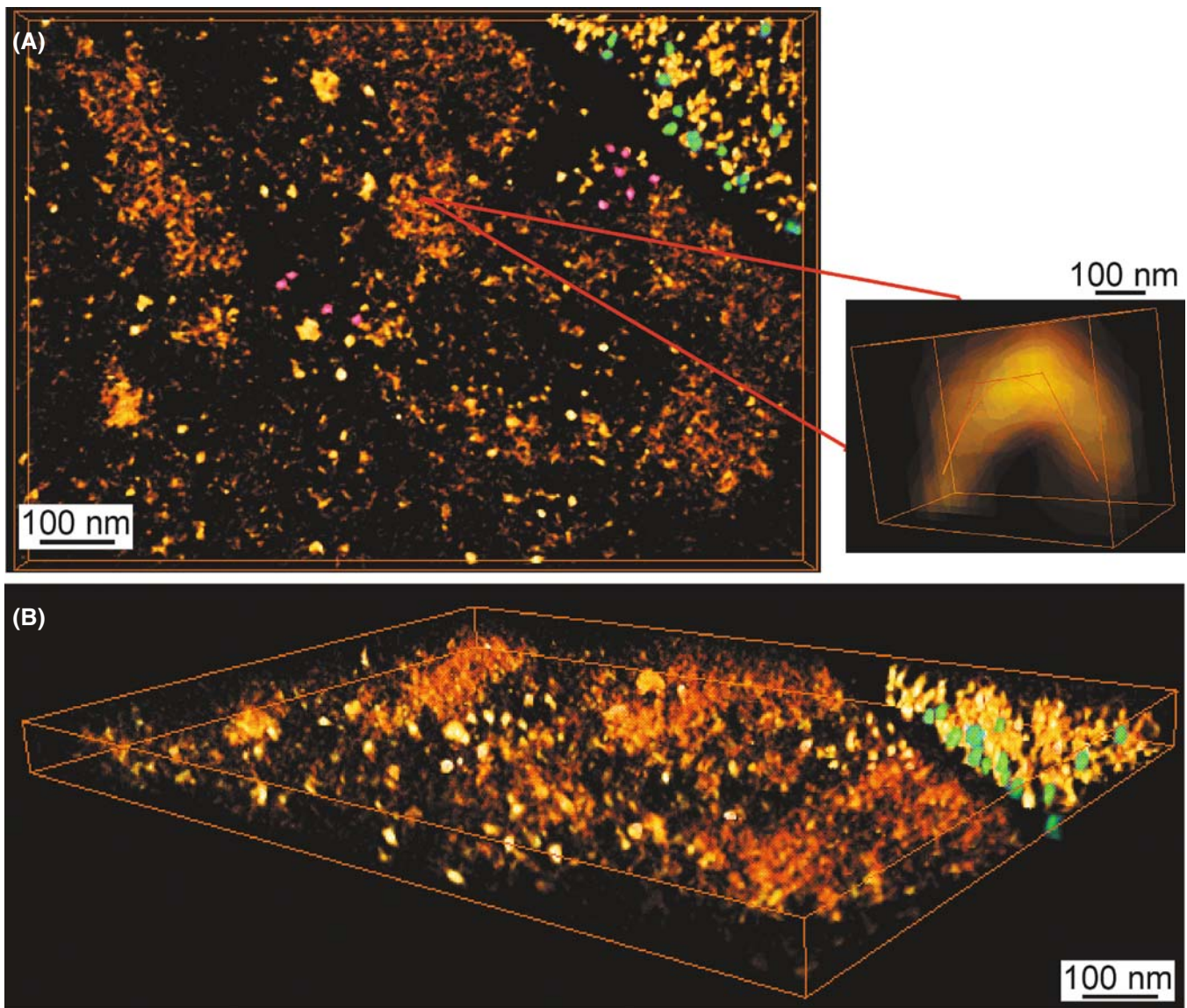
FIGURE 40.15. (A) 2D projection (top view) and (B) energy-filtered, 3D-tomographic image reconstructed from multiple P-L$_{2,3}$ edge filtered images showing the phosphorus distribution in an unstained plastic section of freeze-substituted *Drosophila* larva. The principal region is part of a cell nucleus and the top right is a region of cytoplasm containing ribosomes. The phosphorus distribution reflects the distribution of nucleic acid. Ribosomes (colored green) are known to contain about 7000 P atoms in their RNA. Another series of phosphorus-containing dense particles of unknown origin are present in the nucleus (see enlarged inset).

from a set of 2D projections. (See the paper by Midgley and Weyland.) Because ionization-edge composition images are not susceptible to significant contrast changes as a function of tilt, they are ideal for tomographic reconstruction which reveals the surface features, growth angles/facets, and other features that are not easily obtained from the usual 2D projection image. EFTEM tomography is similar to XEDS tomography which we didn't discuss: EFTEM tomography has the advantage of much quicker generation because XEDS tomography is only feasible via a series of tilted STEM images which take much longer to produce.

Figure 40.15A shows one of the P-L ionization-edge images from a tilt series and Figure 40.15B shows the reconstructed tomographic image of the distribution of P in a cell from a fruit fly. In this area, the biologists are well ahead of the materials scientists and Leapman et al., in 2004, gave a fine example of the application of EELS tomography to discerning the 3-D shape of ribosomes (not quite EELS of eels, but of nematode worms, which look a bit like eels!). In contrast to ionization-edge images, plasmon images retain significant diffraction contrast and so are less useful for tomography.

EFTEM tomography is an area that will see increasing applications, particularly as nanotechnologists pursue their dream of manufacturing devices in a controlled manner from the atom/molecule upward. The ability of EFTEM (and to a lesser extent, XEDS) to reveal the actual shape (combined with the quantitative local chemistry) of quantum dots, gate oxides, and other sub-nanometer fabrications will seriously enhance TEM's role in this growing field.

The ability to extract 3D information by tomographic methods is just one of several examples of the extraordinary advances that have taken place in the TEM field since the first edition of this book was published more than 10 years ago.

It is worth concluding now, as we did then, that we encourage you to experiment with your TEM at all opportunities and never think that there is nothing new to discover. The current generation of students growing up with an expectation of, and familiarity with, full computer control of everything and access to information immediately from anywhere should be able to combine these skills to make TEMs perform in ways that the former generation of more manually oriented TEM operators could never dream of. For example, we haven't even mentioned time-resolved EELS although the strong low-loss signal and efficient collection means that gathering spectra with millisecond or even microsecond resolution is not out of the question and ultra-fast (nanosecond) TEM imaging using laser-excited sources is fast becoming a reality. No doubt there will be a serious need for yet another edition of 'TEM: a text for nanotechnologists' a decade hence, which we sincerely hope will be written by some of those who started their careers by reading this book, rather than by those who wrote it.

CHAPTER SUMMARY

You can appreciate now that there is a wealth of fine detail in the EEL spectrum beyond the relatively strong plasmon peaks and the ionization edges. To extract this information, you need a single-scattering (deconvoluted) spectrum and occasionally some sophisticated mathematical analysis. Interpretation of the data is still limited by our lack of knowledge of the physics of the electron-specimen interactions. However, considerable research is going on into EELS fine-structure studies which are the future of the technique. Both the experimental methods and the theoretical calculations are still developing. We have introduced several specialized topics

- Energy-loss near-edge structure.
- Extended energy-loss fine structure.
- RDF determination.
- Angle-resolved (momentum-transfer) EELS.
- EELS tomography.

However, we have really only given you a suspicion of the potential of these topics. If EELS becomes a technique you use in your research, we recommend watching its development and that of related techniques in the reference sources we have given you in the last four chapters, particularly the quadrennial EELS workshops (see Chapter 37), conferences such as the biannual Frontiers of Electron Microscopy in Materials Science (FEMMS), and the proceedings of the various national and international microscopy and analysis societies which, if you haven't joined by now, you should do so immediately!

BOOKS AND REVIEWS

Brydson, RMD, Sauer, H and Engel, W 2004 *Probing Materials Chemistry using ELNES* in *Transmission Electron Energy Loss Spectrometry in Materials Science and the EELS Atlas* 2nd Ed. 223–270 Ed. CC Ahn Wiley-VCH Weinheim Germany. Comprehensive review of chemical information via the ELNES spectrum; exceptional bibliography.

Egerton, RF 1996 *Electron Energy-Loss Spectroscopy in the Electron Microscope* 2nd edition Plenum Press New York. Everything you need to know on fine structure.

Finnis, MW 2003 *Interatomic Forces in Condensed Matter* Oxford University Press, New York. Essential reading if you are modeling spectra.

Keast, VJ, Scott, AJ, Brydson, R, Williams, DB and Bruley, J 2001 *Electron Energy-Loss Near-Edge Structure – a Tool for the Investigation of Electronic Structure on the Nanometre Scale* J. Microsc. **20** 135–175. Broad-based review with lots of examples.

Koningsberger, DC and Prins, R 1988 *X-Ray Absorption: Principles, Applications, Techniques of EXAFS, SEXAFS and XANES* Wiley New York. Probably more than you'll ever want to know about the X-ray analogs of EELS.

Raether, H 1965 *Electron Energy-Loss Spectroscopy* in Springer Tracts in Modern Physics Springer-Verlag New York. *The* source if you really want to know the physics of EELS.

CALCULATIONS AND TECHNIQUE

Durham, PJ, Pendry, JB and Hodges, CH 1982 *Calculation of X-ray Absorption Near Edge Structure, XANES* Comp. Phys. Comm. **25** 193–205.

Duscher, G, Buczko, R, Pennycook, SJ and Pantelides, ST 2001 *Core-Hole Effects on Energy-Loss Near-Edge Structure* Ultramicrosc. **86** 355–362.

Leapman, RD and Cosslett, VE 1976 *Extended Fine Structure Above the X-ray Edge in Electron Energy Loss Spectra* J. Phys. D: Appl. Phys. **9** L29–L32.

Midgley, PA and Weyland, M 2003 *3D Electron Microscopy in the Physical Sciences: the Development of Z-Contrast and EFTEM Tomography* Ultramicrosc, **96** 413–431.

McBride, W, and Cockayne, DJH 2003 *The Structure of Nanovolumes of Amorphous Materials* J. Non-Cryst. Sol. **318** 233–238.

MOMENTUM TRANSFER STUDIES

Botton, GA, Boothroyd, CB and Stobbs, WM 1995 *Momentum Dependent Energy Loss Near Edge Structures Using a CTEM: the Reliability of the Methods Available* Ultramicrosc. **59** 93–107.

Leapman, RD, Grunes, LA and Fejes, PL 1982 *Study of the L_{23} Edges in the 3d Transition Metals and Their Oxides by Electron-Energy Loss Spectroscopy with Comparisons to Theory*. Phys. Rev. **25**(12) 7157–73.

Leapman, RD and Silcox, J 1979, *Orientation Dependence of Core Edges in Electron-Energy-Loss Spectra from Anisotropic Materials* Phys. Rev. Lett. **42** 1361–1364.

Wang, YY, Cheng, SC, Dravid, VP and Zhang, FC 1995, *Momentum-Transfer Resolved Electron Energy Loss Spectroscopy of Solids: Problems, Solutions and Applications* Ultramicrosc. **59** 109–119.

APPLICATIONS

Alamgir, FM, Jain, H, Williams, DB and Schwarz, R 2003 *The Structure of a Metallic Glass System Using EELFS and EXAFS as Complementary Probes* Micron **34** 433–439.

Batson, PE 1993 *Carbon 1 s Near-Edge-Absorption Fine Structure in Graphite* Phys. Rev. B **48** 2608–2610.

Botton, GA 2005 *A New Approach to Study Bond Anisotropy With EELS* J. Electr. Spectr. Rel. Phen. **143** 129-137.

Botton, GA, Gupta, JA, Landheer, D, McCaffrey, JP. Sproule, GI and Graham, MJ 2002 *Electron Energy Loss Spectroscopy of Interfacial Layer Formation in Gd_2O_3 Films Deposited Directly on Si (001)* J. Appl. Phys. **91** 2921–2924. Bond changes at oxide interfaces.

Bruley, J, Williams, DB, Cuomo, JJ and Pappas, DP 1995 *Quantitative Near-Edge Structure Analysis of Diamond-like Carbon in the Electron Microscope Using a Two-Window Method* J. Microsc. **180** 22–32.

Keast, VJ, Bruley, J, Rez, P, Maclaren, JM and Williams, DB 1998 *Chemistry and Bonding Changes Associated with the Segregation of Bi to Grain Boundaries in Cu* Acta Mater. **46** 481–490.

Leapman, RD, Kocsis, E, Zhang, G, Talbot, TL and Laquerriere, P 2004 *Three-Dimensional Distributions of Elements in Biological Samples by Energy-Filtered Electron Tomography* Ultramicrosc. **100** 115–125.

McComb, DW, Craven, AJ, Hamilton, DA and MacKenzie, M 2004 *Probing Local Coordination Environments in High-k Materials for Gate Stack Applications* Appl. Phys. Lett. **84** 4523–4525.

Muller, DA, Subramanian, S, Batson, PE, Silcox, J and Sass, SL 1996 *Structure, Chemistry and Bonding at Grain Boundaries in Ni_3Al-I. The Role of Boron in Ductilizing Grain Boundaries* Acta Mater. **44** 1637–1645.

Ostanin, S, Craven, AJ, McComb, DW, Vlachos, D, Alavi, A, Paxton, AT and Finnis, MW 2002 *Electron Energy-Loss Near-Edge Shape as a Probe to Investigate the Stabilization of Yttria-Stabilized Zirconia* Phys. Rev. B **65** 224109–117.

Sikora, T, Hug, G, Jaouen, M and Rehr, JJ 2000 *Multiple-Scattering EXAFS and EXELFS of Titanium Aluminum Alloys* Phys. Rev. B **62** 1723–1732.

URLs

1) www.cemes.fr/∼eelsdb
2) www.flapw.de
3) www.physik.uni-augsburg.de/∼eyert/aswhome.shtml
4) www.castep.org
5) http://hermes.phys.uwm.edu/projects/elecstruct/mufpot/MufPot.TOC.html
6) http://feff.phys.washington.edu
7) www.cemes.fr/epsilon/home/main.php

SELF-ASSESSMENT QUESTIONS

Q40.1 Why does the ionization edge extend beyond the critical ionization energy (the edge onset) to give ELNES and EXELFS, rather than exist simply as a peak at the critical ionization energy?

Q40.2 What is the Fermi level/Fermi surface and why is it crucial to our understanding of the energy-loss process?

Q40.3 What is the density of states (DOS) and why are there both filled and unfilled DOS?

Q40.4 Relate the K, L, etc., core shells to the principal quantum numbers (n).

Q40.5 State the Pauli exclusion principle and explain why this is relevant to ELNES.

Q40.6 What is spin-orbit splitting and why is this relevant to ELNES?

Q40.7 What is the dipole-selection rule and why is this relevant to ELNES?

Q40.8 Why does the ionization edge onset for a specific elemental core loss sometimes shift when that element is bonded differently?

Q40.9 What is XANES, how is it detected, and what is its relation to ELNES?

Q40.10 Why do bonding changes change the ELNES?

Q40.11 What useful information is contained in the EXELFS spectrum?

Q40.12 Why is EXELFS such a challenging technique to apply?

Q40.13 What is an exciton?

Q40.14 What is a core hole?

Q40.15 Why is there bonding information in both the low-loss and high-loss spectrum?

Q40.16 Distinguish angle-resolved and spatial-resolved EELS.

Q40.17 Why is angle-resolved EELS linked to the concept of electron momentum transfer?

Q40.18 What is the RDF, why is it useful, and how can you measure it?

Q40.19 Why would you want to calculate the ELNES intensity?

Q40.20 What is Compton scattering and how can we study this in EELS?

Q40.21 Under which circumstance would you choose to use an ELNES spectrum as a fingerprint and what precautions should you take when drawing conclusions from a potential match?

TEXT-SPECIFIC QUESTIONS

T40.1 Distinguish single, multiple, and plural scattering for EELS. How do these definitions compare with scattering terms used in high-resolution imaging?

T40.2 Figure 40.1 gives an electron-wave description of the generation of ELNES and EXELFS. Can you use a particle analogy to describe the process?

T40.3 Is Figure 40.2 drawn for a crystalline metal or an amorphous semiconductor? Explain your answer and thus indicate how the figure would change if the other kind of material were being illustrated.

T40.4 In Figure 40.3 there appears to be no intensity in the ionization edge corresponding to the filled states. Why is this? In a real spectrum there would indeed be intensity before the ionization edge. What would cause this?

T40.5 Why does the Cu L edge in Figures 40.4 and 40.5B exhibit no intense white lines at the edge onset like the rest of the transition metal series in Figure 40.4?

T40.6 In old specimens and older TEMs, the diamond K edge (like in Figure 40.5A) sometimes shows residual intensity preceding the ionization-edge onset, at roughly the same energy as the π^* sp2 peak in the graphite and C_{60} edges shown above. Since diamond has no sp2-bonded carbon, can you speculate what might be giving rise to this intensity?

T40.7 Why are the muffin-tin potential wells in Figure 40.9 symmetric for the metal but asymmetric for the oxide?

T40.8 Look at the comparison of calculated and experimental spectra in Figure 40.10. These calculations were done more than a decade ago. Go on the Web and see if you can find better examples of calculated edge shapes that show a better fit to experimental spectra. If you can't, what conclusions can you draw about calculating ELNES. If you can, what different conclusions can you draw?

T40.9 How do you think that correcting the spherical aberration in the objective lens will improve the study of energy-loss fine structure? Do you think the addition of electron gun monochromators will affect the study of this same phenomenon?

T40.10 What crucial information can be gained about the behavior of semiconductor interfaces and gate oxides via ELNES? (Hint: Google PE Batson and read his papers.)

T40.11 Under what circumstances would you choose an MO rather than an MS approach to calculating the near-edge spectrum?

T40.12 List the principal differences between FLAPW, ASW, CASTEP, and LKKR.

T40.13 ELNES fingerprinting can distinguish different mineral species as in Figure 40.8. Why should we ever bother to use XEDS to study the same problem? Does the beam-sensitivity of many minerals have a role to play in deciding what technique to use? If so, explain what.

T40.14 Why does the signal in Figure 40.12B become noisier at larger wavevectors?

T40.15 Given what you know about the crystal structures of graphite and diamond, would you expect either of their energy-loss spectra to be sensitive to crystallographic orientation? If so, how do you think the fine scale features of the relevant spectrum in Figure 40.5A might change with orientation? (Hint: look at Figure 40.14.)

T40.16 Compare and contrast EXAFS and EXELFS for studying short-range atomic structures. Why would you use EXELFS when TEM diffraction patterns give similar short-range atomic structural information?

T40.17 In addition to ELNES and energy-filtered diffraction for RDF determination, can you think of other ways to explore the structure of glasses using TEM?

T40.18 For both momentum-resolved and tomographic EELS, we have to tilt the specimen considerably. What are the experimental challenges to doing this and how might they be overcome?

T40.19 If the low-loss spectrum reveals the valence states of the atoms in the specimen why do we not use this part of the spectrum more often for bonding studies but instead use ELNES which only explores the unfilled DOS (i.e., the electrons that aren't there)?

T40.20 Explain why K-shell ionization results in a hydrogenic edge.

T40.21 Explain why L shell ionization gives L_1, L_2, and L_3 edges.

T40.22 Why is the L_1 edge rarely visible, thus leaving the usual L edge as the $L_{2,3}$ in spectra from transition metals?

T40.23 Similarly, why is the $M_{4,5}$ edge the expected M edge in the rare earths?

T40.24 Explain why EELS edges and X-ray absorption edges are effectively the same phenomenon.